Available online at www.sciencedirect.com
ScienceDirect
International Journal of Solids and Structures 44 (2007) 8244–8258
INTERNATIONAL JOURNAL OF SOLIDS AND STRUCTURES
www.elsevier.com/locate/ijsolstr

Full field methods and residual stress analysis in orthotropic material. II: Nonlinear approach

Antonio Baldi *

Department of Mechanical Engineering, University of Cagliari, Piazza d'Armi, 09123 Cagliari, Italy

Received 26 November 2006; received in revised form 17 March 2007
Available online 9 June 2007

Abstract

This paper is the second part of a work that analyses the problem of residual stress determination in an orthotropic material by the hole drilling technique combined with full field optical methods. Due to the complex behaviour of the material, two theoretical formulations capable of describing the displacement field in an infinite plate in tension with a hole have been proposed: a simplified one, which can treat only a subset of all orthotropic materials, and a general, much more complex one. In the first part of this work, it has been shown that by using the simplified formulation, it is possible to develop a linear least square approach to the residual stress identification problem capable of treating a large class of orthotropic materials. This second part shows that the same approach can be extended to the general case providing that a somewhat more complex, nonlinear algorithm, is acceptable.

Keywords: Residual stress; Hole drilling; Orthotropic materials; Lekhnitskii's formulation

1. Introduction

This paper is the second part of a work devoted to residual stress measurement in orthotropic materials using the hole drilling approach in combination with full displacement field optical techniques, which, in principle, may provide some advantages with respect to (w.r.t.) the traditional use of strain gauges, in particular higher sensitivity and no-contact measurement.

Residual stress measurement in orthotropic materials has not been widely studied; the best-known work is the one by Schajer (Schajer and Yang, 1994) who, starting from Smith's simplified analysis of the stress field in an orthotropic plate with a hole, developed formulas and correction tables for the hole drilling method in combination with electrical strain gauges. In the optical field, starting from the Smith–Schajer formulas, Cárdenas-García (Cárdenas-García et al., 2005) analysed residual stress for the moiré technique. However, this approach uses a nonlinear formulation that is unnecessarily complex from the numerical standpoint.

* Corresponding author. Tel.: +39 070 675 5707; fax: +39 070 675 5717.
E-mail address: baldi@iris.unica.it

0020-7683/$ - see front matter
doi:10.1016/j.ijsolstr.2007.06.002

Table 1
Characteristic parameters of some materials

Material	E_{11}/E_{22}	ν_{12}	G_{12}/E_{22}	κ	k	m	n
Glass–Epoxy	2.99	0.25	0.5	1.58	1.73	5.48	2.99
Boron–Epoxy	10.0	0.3	0.33	4.65	3.16	29.43	5.98
Graphite–Epoxy	40.01	0.25	0.5	6.29	6.33	79.52	9.60
Oak	2.66	0.32	0.60	1.15	1.63	3.76	2.65
Birch	14.78	0.49	1.06	1.68	3.84	12.93	4.54
Spruce	20.48	0.37	0.77	2.85	4.53	25.82	5.91
Plywood 1	3.86	0.59	0.74	1.02	1.97	3.99	2.82
Plywood 2	24.6	0.3	0.75	3.25	4.96	32.20	6.49
Plywood 3	**1.0**	**0.77**	**2.04**	**−0.53**	**1.00**	**−1.06**	**0.97**
Theo. 1	1.5	0.37	0.4	1.22	1.23	3.0	2.33
Theo. 2	**20.0**	**1.0**	**10.0**	**0.0**	**4.47**	**0.0**	**2.99**
Theo. 3	1.0	0.25	0.05	9.75	1.0	20.0	4.69

κ is Smith's anisotropy index; k, m and n are Lekhnitskii's material parameters. The materials in boldface cannot be analysed using Smith's formulation (Schimke et al., 1968; Savin, 1961; Jones, 1975).

In the first part of this work (Baldi, 2007) a linear least square approach based on Smith's formulation was proposed, showing that the same algorithm used for isotropic materials applies, provided that the Kirsch-related displacement field is replaced by Smith's. However, even though the Smith–Schajer solution is capable of handling a large subset of all orthotropic materials (see Table 1), it is not completely general (it requires $\kappa > 1$); a procedure capable of solving the more difficult cases is developed in this second part, which is organised as follows: Section 2 outlines the full field, linear least square method for orthotropic materials using Smith's formulation as proposed in the first part of this work. Then (Section 3) Lekhnitskii's analytical solution, valid for any orthotropic materials (and any κ), is analysed, showing that (Section 4) it can easily be modified to account for residual stresses. In particular, Section 4.2 shows that the displacement fields in the general orthotropic case do not linearly depend on stress components, and consequently the numerical algorithm in Section 2 cannot be used as is. However, since the basic principle still holds, a new approach, using a nonlinear fit, is developed (Section 5). The estimation of calibration coefficients (in numerical form, using Finite Elements) is analysed in Section 5.1, making it possible to develop a somewhat simpler formulation. In Sections 6 and 7, the developed formulation is tested against numerically generated and experimentally acquired displacement fields. A short discussion closes the paper (Section 8).

2. Linear least square method for orthotropic material

The displacement field at a point j around a hole in an orthotropic plate can be written,[1] in compact form, as (Schajer and Yang, 1994; Cárdenas-García et al., 2005; Baldi, 2007)

$$\begin{aligned} u_x(j) &= a_{11}(j)\sigma_x + a_{12}(j)\sigma_y + a_{13}(j)\tau_{xy} \\ u_y(j) &= a_{21}(j)\sigma_x + a_{22}(j)\sigma_y + a_{23}(j)\tau_{xy} \end{aligned} \tag{1}$$

where the $a_{i,k}$ calibration coefficients depend on material parameters and point location. Eq. (1), which results from Smith's simplified theoretical analysis (Smith, 1944; Schajer and Yang, 1994), requires the material parameter $\kappa = \frac{1}{2}\sqrt{E_{xx}E_{yy}}\left(\frac{1}{G_{xy}} - \frac{2\nu_{xy}}{E_{xx}}\right)$ to be greater than 1, so that it cannot be used for all materials.

Providing Eq. (1) holds, the least square error between ϕ_j, the experimental displacement at point j, and its interpolation can be written as

[1] Since the displacement field is sampled at discrete points, we assume that the data array is sorted, so that it is possible to use a single index j to locate a point.

$$\epsilon = \sum_{j=1}^{N} \{w_j[k_x(j)u_x(j) + k_y(j)u_y(j) - \phi_j]\}^2 \tag{2}$$

where $u_i(j)$ is the component i of the estimated displacement at point j, w_j is normalised measurement reliability at the experimental point or 1 if unknown[2] and the $k_i(j)$ are components of the sensitivity vector (again at point j). Writing u_x and u_y in terms of the stress components, Eq. (2) becomes

$$\epsilon = \sum_{j=1}^{N} \{w_j[(k_x a_{11} + k_y a_{21})\sigma_x + (k_x a_{12} + k_y a_{22})\sigma_y + (k_x a_{13} + k_y a_{23})\tau_{xy} - \phi_j]\}^2 \tag{3}$$

where the explicit dependency on point location of k_i and a_{ij} has been dropped to simplify the notation.

The minimum of the previous expression can easily be determined by differentiating w.r.t. σ_x, σ_y, τ_{xy} and setting the derivatives equal to zero. Writing $\alpha_j = w_j(k_x a_{11} + k_y a_{21})$, $\beta_j = w_j(k_x a_{12} + k_y a_{22})$ and $\chi_j = w_j(k_x a_{13} + k_y a_{23})$ one finally obtains a linear system

$$\begin{pmatrix} \sum_j \alpha_j^2 & \sum_j \alpha_j\beta_j & \sum_j \alpha_j\chi_j \\ & \sum_j \beta_j^2 & \sum_j \beta_j\chi_j \\ \text{symm.} & & \sum_j \chi_j^2 \end{pmatrix} \begin{Bmatrix} \sigma_x \\ \sigma_y \\ \tau_{xy} \end{Bmatrix} = \begin{Bmatrix} \sum_j w_j\alpha_j\phi_j \\ \sum_j w_j\beta_j\phi_j \\ \sum_j w_j\chi_j\phi_j \end{Bmatrix} \tag{4}$$

which allows determination of the best fit parameters (the stress components) of the displacement interpolating functions.

The previous formulation is quite general and does not require a specific form of the displacement fields, providing that they are linearly depend on stress components. The question now is to verify whether this formulation is capable of handling orthotropic materials in the general case. To this end, a brief outline of the properties of orthotropic plates is given below.

3. General solution for the through-hole, orthotropic plate

The through-hole plate issue in the general case of anisotropic material was studied by Lekhnitskii (1963, 1968) and Savin (1961) who adopted different approaches for its solution. Following Schimke et al. (1968) and considering the somewhat simpler case of an orthotropic material, the general biharmonic equation describing the problem is

$$S_{22}\frac{\partial^4\psi}{\partial x^4} + (2S_{12} + S_{66})\frac{\partial^4\psi}{\partial x^2\partial y^2} + S_{11}\frac{\partial^4\psi}{\partial y^4} = 0 \tag{5}$$

where the S_{ij} are the elements of elastic compliance matrix ($S_{11} = 1/E_{11}$, $S_{12} = -\nu_{12}/E_{11}$, $S_{22} = 1/E_{22}$, $S_{66} = 1/G_{12}$). The general solution to Eq. (5) can be written as a combination of four analytic functions ψ_i

$$\psi = \sum_{i=1}^{4} \psi_i(x + \mu_i y) \tag{6}$$

where the μ_i are the solutions of the associated algebraic equation

$$S_{11}\mu^4 + (2S_{12} + S_{66})\mu^2 + S_{22} = 0 \tag{7}$$

that is

$$\mu = \pm\left[\frac{-(2S_{12} + S_{66}) \pm \sqrt{(2S_{12} + S_{66})^2 - 4S_{11}S_{22}}}{2S_{11}}\right] \tag{8}$$

[2] From the statistical point of view, w_j should be $1/\sigma_j$, the inverse of the standard deviation of the measurement at the experimental point j. Usually this datum is not available, however, intensity modulation allows estimation of measurement reliability at each point, so that a weighted summation can be used, even though the resulting covariance matrix will not reflect the actual measurement variance.

It can be shown that Eq. (7) cannot have real roots; on the contrary, double roots are possible, but in this case Eq. (5) can be reduced, by a simple stretch transformation, to $\nabla^4\psi = 0$, which is tantamount to saying that the problem is equivalent to an isotropic one. Thus, Eq. (7) always admits four complex roots, where $\mu_3 = \overline{\mu_1}$ and $\mu_4 = \overline{\mu_2}$, the principal solutions being (Tan, 1988)

$$\mu = \frac{\mathrm{i}}{2}\left(\sqrt{\frac{E_1}{G_{12}} - 2\nu_{12} + 2\sqrt{\frac{E_1}{E_2}}} \pm \sqrt{\frac{E_1}{G_{12}} - 2\nu_{12} - 2\sqrt{\frac{E_1}{E_2}}}\right) \tag{9}$$

where the S_{ij} are expressed in terms of engineering constants.

By introducing two auxiliary variables ($z_1 = x + \mu_1 y$ and $z_2 = x + \mu_2 y$) and the functions $\Gamma_1(z_1) = \partial\psi_1/\partial z_1$ and $\Gamma_2(z_2) = \partial\psi_2/\partial z_2$, it is easy to obtain

$$\begin{aligned}
\sigma_x &= \frac{\partial^2\psi}{\partial y^2} = 2\mathrm{Re}\left[\mu_1^2\frac{\mathrm{d}\Gamma_1}{\mathrm{d}z_1}(z_1) + \mu_2^2\frac{\mathrm{d}\Gamma_2}{\mathrm{d}z_2}(z_2)\right]\\
\sigma_y &= \frac{\partial^2\psi}{\partial x^2} = 2\mathrm{Re}\left[\frac{\mathrm{d}\Gamma_1}{\mathrm{d}z_1}(z_1) + \frac{\mathrm{d}\Gamma_2}{\mathrm{d}z_2}(z_2)\right]\\
\tau_{xy} &= -\frac{\partial^2\psi}{\partial x\partial y} = -2\mathrm{Re}\left[\mu_1\frac{\mathrm{d}\Gamma_1}{\mathrm{d}z_1}(z_1) + \mu_2\frac{\mathrm{d}\Gamma_2}{\mathrm{d}z_2}(z_2)\right]
\end{aligned} \tag{10}$$

while the displacement field can be written (neglecting rigid body terms) as

$$\begin{aligned}
u &= 2\mathrm{Re}[p_1\Gamma_1(z_1) + p_2\Gamma_2(z_2)]\\
v &= 2\mathrm{Re}[q_1\Gamma_1(z_1) + q_2\Gamma_2(z_2)]
\end{aligned} \tag{11}$$

p_1, p_2, q_1 and q_2 being complex functions of the material properties only ($p_i = \mu_i^2 S_{11} + S_{12}$, $q_i = S_{22}/\mu_i + \mu_i S_{12}$, $i = 1,2$).

Taking into account the boundary conditions—a uniform stress P at ∞, inclined by φ w.r.t. the X principal axis—it can be shown that the Γ_i functions can be written as

$$\begin{aligned}
\Gamma_1 &= A_L z_1 + \sum_{k=1}^{\infty} A_k \xi_1^{-k}\\
\Gamma_2 &= B_L z_2 + \sum_{k=1}^{\infty} B_k \xi_2^{-k}
\end{aligned} \tag{12}$$

where A_L and B_L depend on the stress value at infinity and its orientation, the summations represent the local corrections around the hole with respect to the unperturbed stress field and the ξ_i functions result from inverse mapping of the exterior of the unit circle in the ξ_i plane onto the exterior of the ellipse $z_i = \cos\theta + \mu_i \sin\theta$ in the z_i plane.

Noting that along the edge of the opening the inverse mapping reduces to $\xi_i^{-1} = \mathrm{e}^{-\mathrm{i}\theta}$, it is easy to show (Lekhnitskii, 1968) that the tangential stress σ_θ around a circular hole (where obviously σ_r is null) is

$$\begin{aligned}
\sigma_\theta = P\frac{E_\theta}{E_1}\{&[-\cos^2\varphi + (k+n)\sin^2\varphi]k\cos^2\theta + [(1+n)\cos^2\varphi - k\sin^2\varphi]\sin^2\theta - n(1+k+n)\\
&\times \sin\varphi\cos\varphi\sin\theta\cos\theta\}
\end{aligned} \tag{13}$$

where E_θ is Young's modulus in the tangential direction and the k, n and m parameters depend on the material properties and are closely related to μ_i ($k = -\mu_1\mu_2 = \sqrt{E_1/E_2}$, $m = E_1/G_{12} - 2\nu_{12}$, $n = \sqrt{2k+m}$).

Note that Eq. (13) only holds at the hole boundary. On the contrary, it is not possible to obtain real-value analytical functions inside the plate. Thus, the displacements (stresses) have to be estimated numerically, taking care to select the right solution branch and to avoid complex square root singularities (see Appendix A for details).

4. Residual stress

Using Eqs. (10)–(12) it is possible to determine the displacement and stress fields for residual stress. In fact, hole drilling can be viewed as the subtraction of the solution for the through-hole plate loaded by a couple of uniform stress at ∞ from that for the hole-free, loaded plate. This idea will be applied in the following sections: first the case of the single load will be studied, then its solution will be extended to the general, using the superposition principle.

4.1. Single load

Bearing in mind that the Γ_i functions (Eq. (12)) result from the contribution of two terms—the unperturbed stress field due to loads at infinity and a local correction due to the presence of the hole—the residual stress solution can be obtained from Eq. (12) by setting A_L and B_L to zero.

$$\begin{aligned}\Gamma_1 &= \sum_{k=1}^{\infty} A_k \xi_1^{-k} \\ \Gamma_2 &= \sum_{k=1}^{\infty} B_k \xi_2^{-k}\end{aligned} \tag{14}$$

The final solution can be obtained by truncating the summations to the first term, so that A_1 and B_1 become

$$\begin{aligned}A_1 &= -\frac{P}{2(\mu_1-\mu_2)}[\mathrm{i}\cos^2\varphi - \mu_2 \sin^2\varphi - (1-\mathrm{i}\mu_2)\sin\varphi\cos\varphi] \\ B_1 &= -\frac{P}{2(\mu_2-\mu_1)}[\mathrm{i}\cos^2\varphi - \mu_1 \sin^2\varphi - (1-\mathrm{i}\mu_1)\sin\varphi\cos\varphi]\end{aligned}$$

By simple algebra it can be shown that in this case Eq. (11) reduces to

$$\begin{aligned}u &= 2P\,\mathrm{Re}\left[\delta_1\left(\frac{p_1\delta_2}{\xi_1} - \frac{p_2\delta_3}{\xi_2}\right)\right] \\ v &= 2P\,\mathrm{Re}\left[\delta_1\left(\frac{q_1\delta_2}{\xi_1} - \frac{q_2\delta_3}{\xi_2}\right)\right]\end{aligned} \tag{15}$$

where δ_1, δ_2 and δ_3 are complex functions of material and load orientation.

$$\begin{aligned}\delta_1 &= (\sin\varphi - \mathrm{i}\cos\varphi)/[2(\mu_1-\mu_2)] \\ \delta_2 &= \cos\varphi + \mu_2\sin\varphi \\ \delta_3 &= \cos\varphi + \mu_1\sin\varphi\end{aligned} \tag{16}$$

Figs. 1 and 2 show the u and v displacement fields around the hole for the through-hole and residual stress in the case of single loading. Even though they look quite different, in effect they only differ in the z-proportional term. On the contrary, the stress fields are qualitatively equivalent since they differ by a linear term.

4.2. Two principal stresses

Taking into account the previous section and two principal stresses σ_1 and σ_2 at infinity, with angle φ and $\varphi + \pi/2$ w.r.t. the material's principal axis (X) and using the superposition principle, the u and v displacements can be written as

$$\begin{aligned}u &= a\sigma_1 + b\sigma_2 \\ v &= c\sigma_1 + d\sigma_2\end{aligned} \tag{17}$$

where a, b, c and d are calibration coefficients

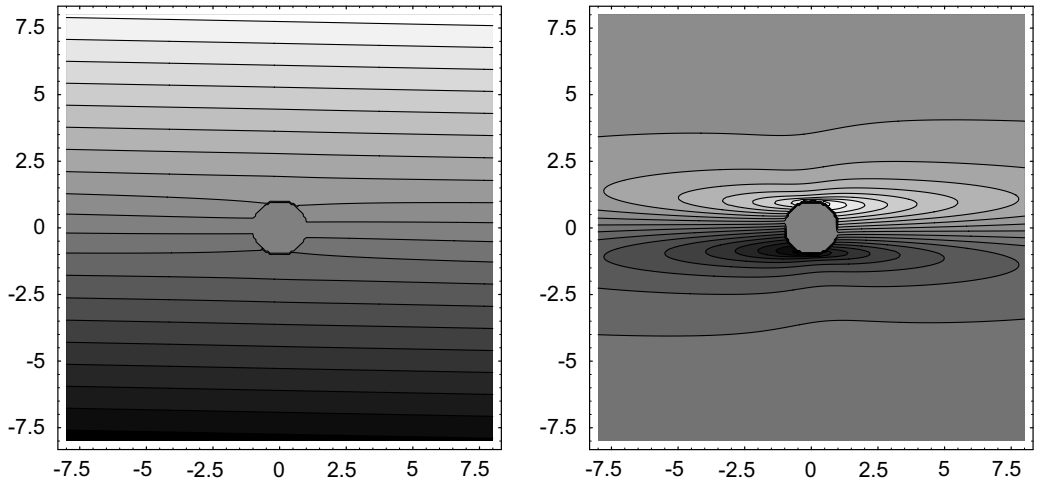

Fig. 1. u displacement field related to a 45° inclined load in an orthotropic graphite/epoxy plate. Left: through-hole. Right: residual stress.

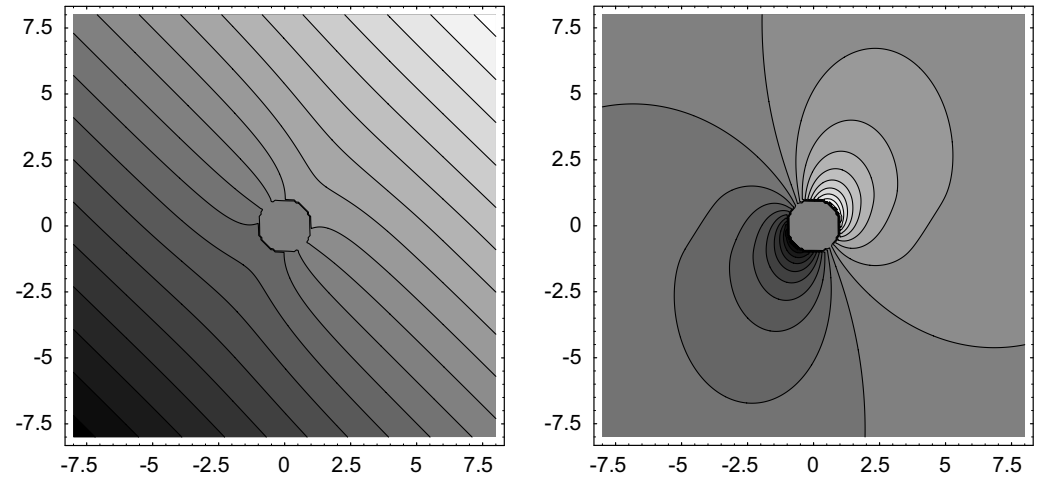

Fig. 2. v displacement field related to a 45° inclined load in an orthotropic graphite/epoxy plate. Left: through-hole. Right: residual stress.

$$a = 2\mathrm{Re}\left[\delta_1\left(\frac{p_1\delta_2}{\xi_1} - \frac{p_2\delta_3}{\xi_2}\right)\right] \quad b = 2\mathrm{Re}\left[\delta_4\left(\frac{p_1\delta_5}{\xi_1} - \frac{p_2\delta_6}{\xi_2}\right)\right]$$
$$c = 2\mathrm{Re}\left[\delta_1\left(\frac{q_1\delta_2}{\xi_1} - \frac{q_2\delta_3}{\xi_2}\right)\right] \quad d = 2\mathrm{Re}\left[\delta_4\left(\frac{q_1\delta_5}{\xi_1} - \frac{q_2\delta_6}{\xi_2}\right)\right] \tag{18}$$

and δ_4–δ_6 can be obtained from Eq. (16) by substituting $\varphi + \pi/2$ for φ

$$\begin{aligned}\delta_4 &= (\cos\varphi + \mathrm{i}\sin\varphi)/[2(\mu_1 - \mu_2)]\\ \delta_5 &= \mu_2\cos\varphi - \sin\varphi\\ \delta_6 &= \mu_1\cos\varphi - \sin\varphi\end{aligned} \tag{19}$$

Eqs. (17)–(19) could in principle replace the u and v displacements in Eq. (2). In fact, Eqs. (17) can also be written

$$u = \frac{a+b}{2}(\sigma_1 + \sigma_2) + \frac{a-b}{2}(\sigma_1 - \sigma_2)$$

$$v = \frac{c+d}{2}(\sigma_1+\sigma_2) + \frac{c-d}{2}(\sigma_1-\sigma_2)$$

or, in terms of σ_x, σ_y and τ_{xy}, as

$$\begin{aligned} u &= \frac{a+b}{2}(\sigma_x+\sigma_y) + \frac{a-b}{2}[(\sigma_x-\sigma_y)\cos(2\varphi) + 2\tau_{xy}\sin(2\varphi)] \\ &= A(\sigma_x+\sigma_y) + B[(\sigma_x-\sigma_y)\cos(2\varphi) + 2\tau_{xy}\sin(2\varphi)] \\ v &= \frac{c+d}{2}(\sigma_x+\sigma_y) + \frac{c-d}{2}[(\sigma_x-\sigma_y)\cos(2\varphi) + 2\tau_{xy}\sin(2\varphi)] \\ &= C(\sigma_x+\sigma_y) + D[(\sigma_x-\sigma_y)\cos(2\varphi) + 2\tau_{xy}\sin(2\varphi)] \end{aligned} \tag{20}$$

Thus, using this formulation, u and v seem to be exactly the same as the isotropic case. However, this similarity is only formal; in fact, for isotropic materials displacements are written in a cylindrical coordinates system—so that φ is a variable determining the point position, i.e. it is a known parameter—while Eqs. (20) use rectangular coordinates and the point position is defined by the x and y variables (hidden inside the ξ_1 and ξ_2 auxiliary variables). In this case φ determines the angle between the first principal stress and the material's X axis so that it is actually unknown. In conclusion, the a–d parameters (the equivalent of A–G coefficients in the isotropic case), are not really constant but depend on residual stress orientation, so that the linear dependency of displacements on stress components required by the algorithm of Section 2 is not fulfilled.

5. Nonlinear least square method for orthotropic material

Even though the linear least square formulation in Section 2 cannot be directly used, the general approach—by adjusting the parameters of the theoretical displacement field to fit the experimental data—still holds, provided one accepts solving a nonlinear system. In fact, once the material parameters and the point of interest are defined, the a–d parameters are known functions, so that both the displacement projected in the sensitivity direction and its partial derivatives w.r.t. stress components can be analytically estimated

$$f = k_x u + k_y v = k_x(a\sigma_1 + b\sigma_2) + k_y(c\sigma_1 + d\sigma_2) \tag{21}$$

$$\begin{aligned} \frac{\partial f}{\partial \sigma_1} &= a k_x + c k_y \\ \frac{\partial f}{\partial \sigma_2} &= b k_x + d k_y \\ \frac{\partial f}{\partial \varphi} &= \mathrm{Re}\left\{ e^{2i\varphi} \frac{i(k_x p_2 + k_y q_2)(i+\mu_1)\xi_1}{2(\mu_1-\mu_2)\xi_1\xi_2} + \frac{(k_x p_1 + k_y q_1)(1-i\mu_2)\xi_2}{2(\mu_1-\mu_2)\xi_1\xi_2} \right\}(\sigma_1-\sigma_2) \end{aligned} \tag{22}$$

where the a–d parameters have been expanded in the third equation only and the explicit dependency on j has been dropped to simplify the notation.

The resulting system is clearly nonlinear, since the third derivative contains mixed terms of the form $\sigma_1\sin(\varphi)$, …, $\sigma_2\cos(\varphi)$, so that to solve the fitting problem one has to use a nonlinear fitting algorithm such as that of Levemberg–Marquard (Press et al., 1992) or similar.

Levemberg–Marquard algorithm uses an iterative, gradient-descendant approach so that, given the current set of fitting parameters, it only needs the value of the fitting function (Eq. (21)) and its local derivatives w.r.t. the fitting parameters (Eq. (22)) to estimate the next candidate set. Thus, the residual stress problem in orthotropic material can be solved even in the general case, even though a somewhat more complex procedure is required. However, this is not a great obstacle: Levemberg–Marquardt algorithm is well known and usually available as a library function, so that users have only to write a function estimating Eqs. (21) and (22) for a given set of parameters and point location.

One point to note is that the nonlinear fit algorithms are intrinsically iterative, so that they need a starting point sufficiently close to the correct solution to ensure convergence. To solve this problem one can either use predefined/randomly chosen values or use an isotropic algorithm (Baldi, 2005) to obtain a rough estimate of the solution (we are implicitly assuming that due to the material parameters the formulation of Section 2 cannot be used).

5.1. Simplified numerical procedure: calibration coefficients

Eqs. (21) and (22) are quite difficult to implement: in fact, all computations have to be performed using complex numbers and the results (the real part of the estimated quantities) is obtained as the last operation of a long series of steps; moreover, estimating the $a, \ldots, d$ coefficients involves knowing ξ_1 and ξ_2, whose evaluation requires special attention (see Appendix A).

However, most of the complexities come from the rather intricate dependency of the $a, \ldots, d$ parameters on material properties and point location; therefore, one can expect that by taking apart these factors, the relation between the parameters and the principal stress orientation φ is a much simpler function. Actually, looking at the way δ_1, δ_2 and δ_3 combine in $a, \ldots, d$, it is evident that apart from constant terms, the $a, \ldots, d$ parameters behave like $\sin(2\varphi)$. Fig. 3, showing the $a, \ldots, d$ parameters at a random location near the hole, confirms this behaviour (the material parameters correspond to the first entry of Table 1). Moreover, it also confirms that mean value, amplitude and phase shift strongly depend on material properties and point location and cannot be known *a priori*. Fig. 4 strengthens this assertion: in fact, it shows how the a parameter, estimated at a fixed point (the same as in the previous figure), varies depending on the material.

In any case, the sinusoidal behaviour is confirmed in all cases so that if for each point we are able to identify the parameters of the sinusoid, we can write $a, \ldots, d$ in a much simpler form

$$\begin{aligned} a(x,y,\varphi,\mu_1,\mu_2) &= a_m + a_\gamma \cos(\theta + a_\theta) \\ b(x,y,\varphi,\mu_1,\mu_2) &= a_m + a_\gamma \cos(\theta + a_\theta + \pi/2) \\ c(x,y,\varphi,\mu_1,\mu_2) &= c_m + c_\gamma \cos(\theta + c_\theta) \\ d(x,y,\varphi,\mu_1,\mu_2) &= c_m + c_\gamma \cos(\theta + c_\theta + \pi/2) \end{aligned} \tag{23}$$

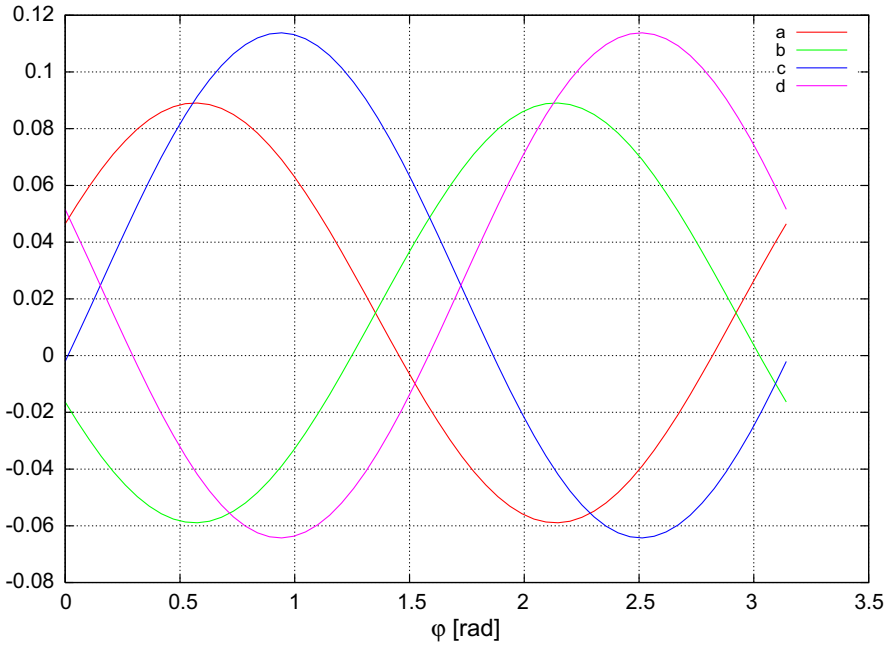

Fig. 3. The a, b, c and d parameters as a function of load orientation. Point coordinates are $x = 5$, $y = 3.4$ while the material properties are taken from the first row of Table 1.

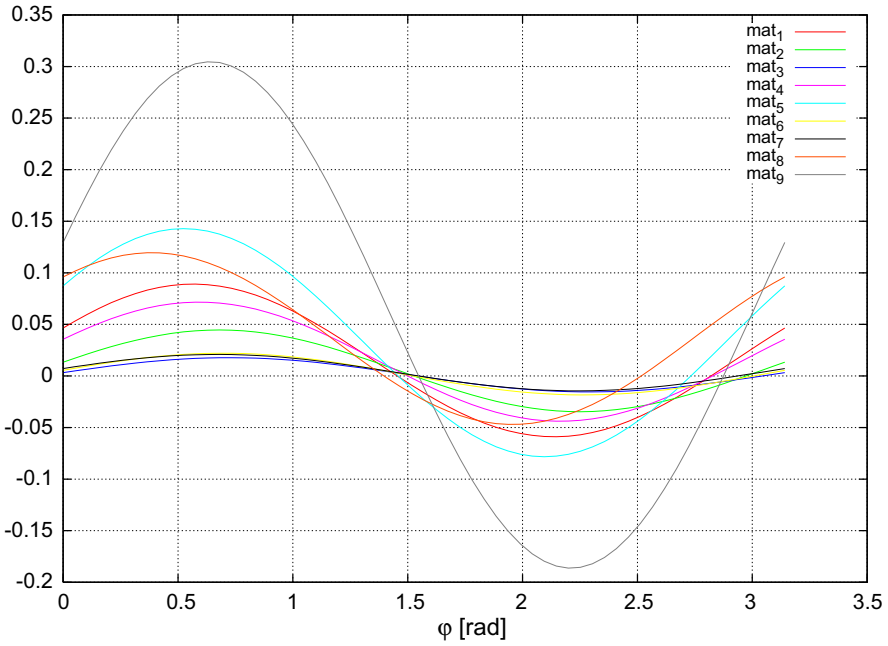

Fig. 4. The a parameter as a function of load orientation. Each curve corresponds to a different material, taken from Table 1, while point location is the same as in the previous picture ($x = 5$, $y = 3.4$). Note that the parameters of the sinusoid (mean value, modulation and initial phase) change from one material to another.

where two triples of real coefficients a_m, a_γ, a_θ and c_m, c_γ, c_θ have been introduced instead of the complex δ_1, δ_2, δ_3, …, μ_2 parameters used by the original formulation. a_m, a_γ, a_θ (c_m, c_γ, c_θ) obviously correspond to the mean value, the modulation and the phase shift of the sinusoid; the auxiliary angular variable $\theta = 2\varphi$ has been introduced to simplify the subsequent analysis.

Eq. (23) takes into account the φ dependency only, so that one could object that the new parameters depend on point location and material properties. Actually this is true, but, as will be shown below, they can be evaluated in a simple way using FEM analysis.

This alternative formulation makes clear the main difference between orthotropic and isotropic materials: the dependency of calibration coefficients on residual stress orientation; moreover, it is computationally much simpler than the previously described approach (Eq. (22)). In fact, the a, …, d parameters required by Eq. (21) are now evaluated using Eq. (23) and not by means of the long calculations required by Eqs. (17)–(19); the partial derivatives of the projected displacement with respect to stress components are also simpler and can be written as

$$\begin{aligned}
\frac{\partial f}{\partial \sigma_1} &= a k_x + c k_y \\
\frac{\partial f}{\partial \sigma_2} &= b k_x + d k_y \\
\frac{\partial f}{\partial \varphi} &= -\{a_\gamma k_x [\sin(\varphi + a_\varphi)\sigma_1 + \cos(\varphi + a_\varphi)\sigma_2] + c_\gamma k_y [\sin(\varphi + c_\varphi)\sigma_1 + \cos(\varphi + c_\varphi)\sigma_2]\}
\end{aligned} \tag{24}$$

where the first two lines are formally the same as Eq. (22), but actually simpler because a, …, d have to be evaluated using Eq. (23).

5.2. FEM estimation of calibration coefficients

Estimating the parameter of a sinusoidal function—mean value, modulation and phase shift—is a well known problem in the optical interferometry field. The standard solution is given by the so-called "phase shift-

ing algorithms" (Creath, 1993) which consist of adding known quantities to the phase, successively estimating (via a linearised least square approach) the function parameters based on its sampled values. Several algorithms have been proposed, mainly to improve their robustness with respect to shift errors, but in any case a minimum of three acquisitions are required.

In the case of residual stress, adding a phase shift corresponds to changing the load orientation; moreover, since the b and d coefficients are actually $\pi/2$ shifted versions of a and c, no extra parameters related to them have to be considered and only a single load has to be applied for each orientation. Thus, we have to perform a certain number of FEM simulations (depending on the selected phase shifting algorithm), using a predefined set of load orientations, and then using the resulting u displacements as input to estimate the coefficients of a, and the v displacements to estimate c.

Since we are performing a numerical simulation, we expect no phase shift error (load orientation error), so that we can use the simpler phase shifting algorithm (that is, the three image, 90° algorithm). The standard formulation for this case expects $\pi/4$, $3\pi/4$ and $5\pi/4$ phase shifts and returns a $\pi/4$ shifted initial phase. A more convenient sequence is 0, $\pi/2$, π (which implies 0, $\pi/4$ and $\pi/2$ oriented loads) and a 0-shifted initial phase. The related formulas can easily be estimated using standard treatment such as

$$\begin{aligned} a_m &= (u_1 + u_3)/2 \\ a_\gamma &= 1/2\sqrt{(u_1 - 2u_2 + u_3)^2 + (u_3 - u_1)^2} \\ a_\theta &= \arctan[(u_1 - 2u_2 + u_3)/(u_1 - u_3)] \end{aligned} \tag{25}$$

where u_1, u_2 and u_3 obviously correspond to the FEM-evaluated u displacements for the first, second and third load orientations while c_m, c_γ and c_θ can be estimated by replacing the v_i components in the same formulas.

Note that since a $\pi/4$ oriented load has to be applied, it is not possible to use a quarter-of-a-circle mesh, so a full circular mesh has to be built. Actually in the through-hole case we are analysing, it is quite difficult to constrain the centre of the hole. A solution to this problem can be obtained by reversing the boundary condition scheme by applying an equivalent load on the hole boundary and constraining the outer part of the

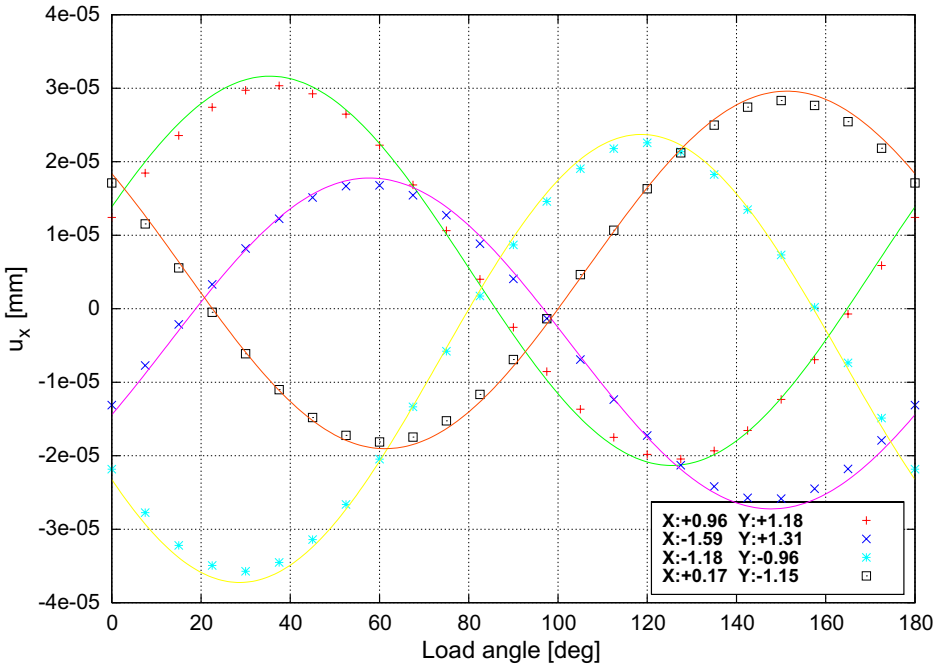

Fig. 5. u displacement of four points around the hole as a function of load angle. Continuous lines are theoretically estimated using Eq. (15), while the points are from Finite Element calculations (plane stress).

disk. Recalling that in a hole drilling test one starts from a uniform stress field to successively perform the drilling, it is quite easy to show (using Mohr's circle) that the radial and tangential pressure terms that have to be applied on the hole side are

$$\sigma_r = -p/2[1 + \cos(2\alpha - 2\varphi)]$$
$$\tau_{r\theta} = -p/2 \sin(2\alpha - 2\varphi)$$

which eventually have to be integrated and projected on the X and Y axes to obtain nodal loads. Note that while α is the angular coordinate, the actual rotation in the Mohr plane is $2(\alpha - \varphi)$ to allow for load orientation.

Fig. 5 compares the analytically estimated $u(\varphi)$ displacement (using Eq. (15)) with the values determined using the Finite Element Method at four nodes around the hole. As expected, the Finite Element solution slightly underestimates the displacement due to the finite size of the mesh ("infinite" elements have not been used). Note the sinusoidal behaviour of the functions (due to a, …, d coefficients) and that phase shifting depends on the point position.

6. Numerical tests

The same numerical tests performed in the first part of this work for the linear algorithm (Baldi, 2007) were repeated using the nonlinear fit proposed in Section 5. In fact, the new formulation is completely general, so that it is able to handle any orthotropic material; moreover, by comparing the results of both algorithms, it is simpler to detect specific problems. The displacement fields to be analysed were generated using a FEM program (MSC Marc 2005r2), to later perturb them by adding Gaussian distributed noise with zero mean and standard deviation equal to 0%, 5% and 10% of maximum displacement. Considering the fast decay of the signal, this means that as soon as we move a few diameters from the centre, noise completely shadows the information contents. Thus, the results should have an increasing standard deviation, with no bias (we are using a zero mean distribution).

Figs. 6 and 7 show the results obtained with both the nonlinear and linear algorithms. In particular, Fig. 6 shows the results obtained using the 5% standard deviation, while in Fig. 7 the noise factor is 10%. It should be noted that noise in the X and Y direction is not correlated (that is, the u and v fields have been perturbed separately) so that we should not expect similar results for the same load. Tests have been performed using a single load oriented at 0°, 15°, 30°, …, 90° from the X axis using a 100 MPa residual stress level; loads were applied on the hole side while the outer circle was tangentially constrained. Since the linear algorithm estimates the stress components in terms of σ_x, σ_y, τ_{xy}, to compare its results with the nonlinear algorithm the principal stresses and their orientation were estimated using standard formulas.

Looking at the figures, it is apparent that the performances of both algorithms (linear and nonlinear least square fit) are quite the same: it never occurs that the linear algorithm gives very good results and the nonlinear algorithm gives very bad ones (and vice versa). Even when considering a 10% noise level, results are very good, showing only a somewhat larger error band.

It is worth noting that the results of the isotropic algorithm (used to estimate the starting guess of the nonlinear algorithm) may be quite wrong, giving principal stresses up to 10 times larger than the correct ones (for example, the starting guess for the 30° load, with no noise, is $\sigma_1 = 1196.1$ MPa, $\sigma_2 = -328.6$ MPa, $\varphi = 44.3°$). This implies that even when, as in this case, Smith's orthotropy index κ is not very large ($\kappa = 3.25$), the isotropic algorithm should not be used to estimate residual stress level in orthotropic materials (the material parameters used during the tests were $E_1 = 93.7$ GPa, $E_2 = 7.45$ GPa, $\nu_{12} = 0.26$, $G_{12} = 3.98$ GPa).

Fig. 8 shows that the nonlinear algorithm gives similar results even when applied to materials which cannot be analysed using the Smith–Schajer theory. The noise factor used during the calculation was $\sigma = 5\%$ of maximum displacement and material parameters were $E_{11} = 76.24$ GPa, $E_{22} = 28.09$ GPa, $\nu_{12} = 0.879$, $G_{12} = 35.82$ GPa, $\kappa = 0.11$, which have been evaluated using the classical lamination theory for a graphite/epoxy laminate (lamina parameters: $E_{11} = 206.84$ GPa, $E_{22} = 5.17$ GPa, $\nu_{12} = 0.25$, $G_{12} = 2.59$ GPa, Jones, 1975) and the simple sequence $(0/45/-45)_s$.

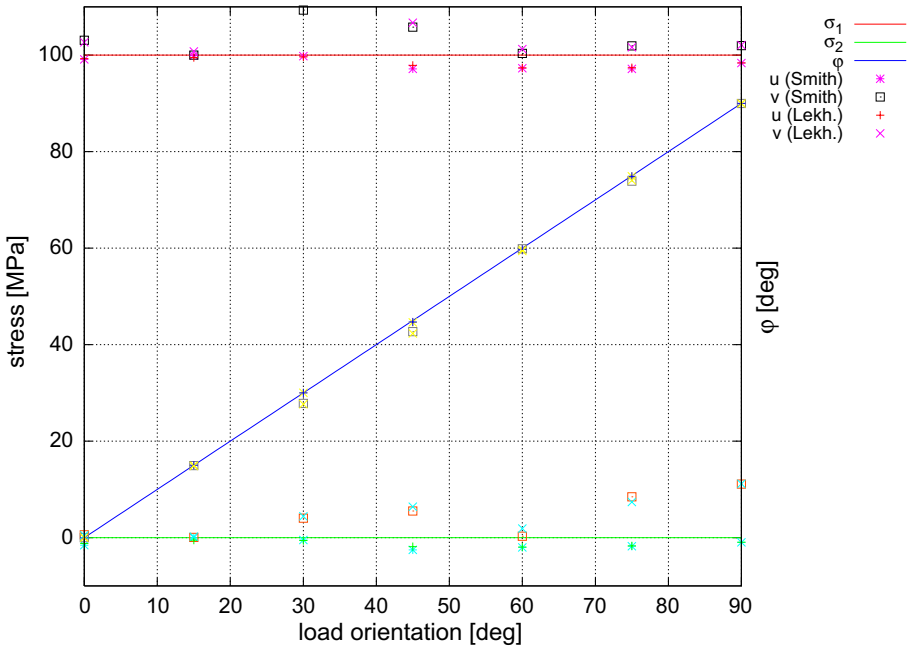

Fig. 6. Estimated residual stress using the linear and nonlinear algorithms. The expected result is $\sigma_1 = 100$ MPa, $\sigma_2 = 0$. u and v displacement fields have been perturbed by adding a Gaussian noise with 0 mean and standard deviation equal to 5% of maximum displacement.

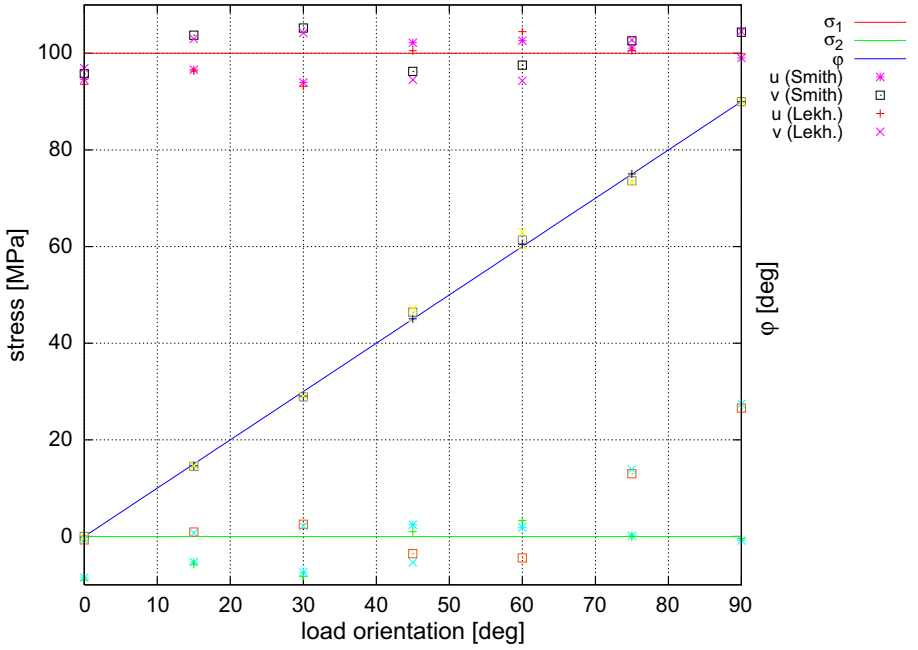

Fig. 7. Estimated residual stress using the linear and nonlinear algorithms. The expected result is $\sigma_1 = 100$ MPa, $\sigma_2 = 0$. u and v displacement fields have been perturbed by adding a Gaussian noise with 0 mean and standard deviation equal to 10% of maximum displacement.

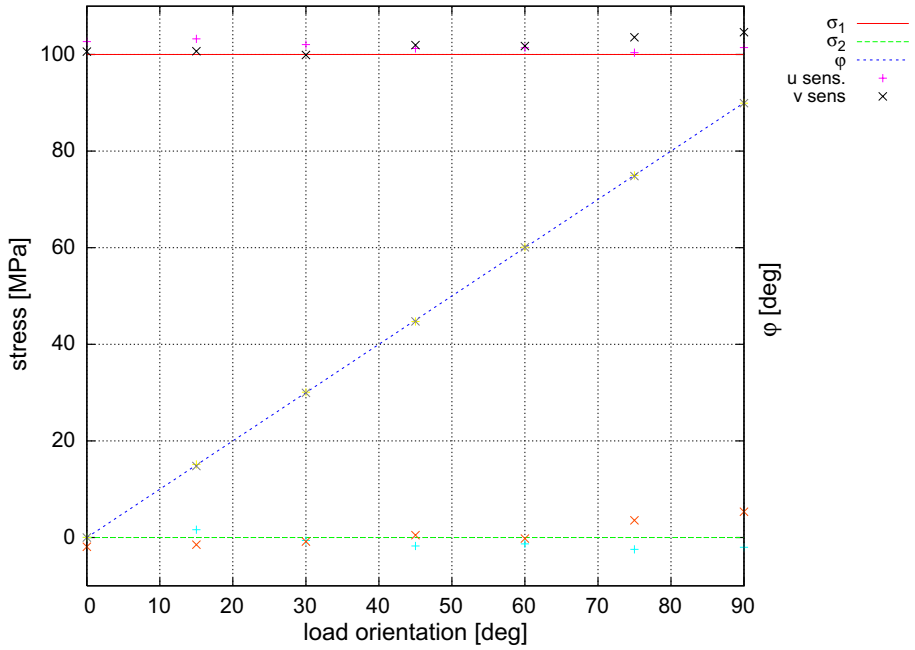

Fig. 8. Estimated residual stress using the nonlinear algorithm on a material which cannot be analysed using the Smith–Schajer theory. The expected result is $\sigma_1 = 100$ MPa, $\sigma_2 = 0$. u and v displacement fields have been perturbed by adding a Gaussian noise with 0 mean and standard deviation equal to 5% of maximum displacement.

7. Experimental tests

The same experimental procedure described in the first part of this work (Baldi, 2007) can be used to test the nonlinear algorithm. A unidirectional graphite/peek laminate ($E_{11} = 133.8$ GPa, $E_{22} = 8.9$ GPa, $\nu_{12} = 0.3$, $G_{12} = 5.1$ GPa, $\kappa = 6.61$) was drilled (to relax internal residual stresses) and then loaded. The displacement field thus obtained around the hole was acquired using an in-plane sensitivity speckle interferometry setup, with a He–Ne laser ($\lambda = 632.8$ nm), an illumination angle of $\theta = 30°$ and X sensitivity.

To obtain the residual stress field, the linear displacement field related to a hole-free orthotropic plane was estimated (obviously after masking the area around the hole) and numerically subtracted from the original data. Figs. 9 and 10 show the phase modulo 2π relating to two different load steps before and after linear term removal. It should be noted that the large displacements related to the loading procedure limit the stress level (due to in-plane decorrelation) thus making the test more difficult than a real residual stress measurement. In any case, the expected results for the two steps were $\sigma_x = 7$ and $\sigma_x = 8.45$ MPa, while the estimated residual stress, by the nonlinear procedure were $\sigma_1 = 7.8$ and $\sigma_1 = 9.2$, showing a good agreement with the linear fit algorithm.

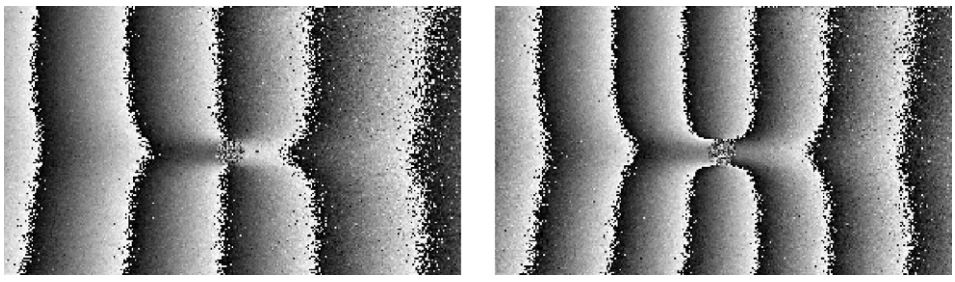

Fig. 9. Phase modulo 2π around the hole at two successive load steps. Note the linear term due to the external load.

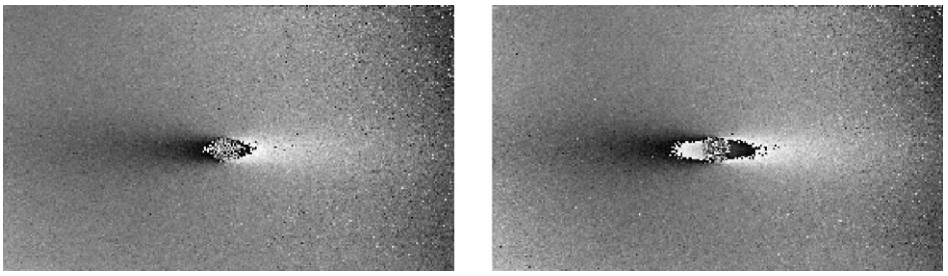

Fig. 10. Phase modulo 2π around the hole after linear term removal.

8. Conclusions

Determining residual stresses in orthotropic materials is much more difficult than in isotropic materials as the dependency of the calibration coefficients on load orientation makes all the algorithms developed so far unfeasible. However, in the first part of this work it was shown that using the Smith–Schajer formulation, a large subset of orthotropic materials can be analysed using a standard linear least square fitting algorithm. The general case, discussed in this paper, requires a somewhat more complex procedure, but the residual stress identification problem can still be solved, provided appropriate calibration functions are available. Because of the nature of orthotropic materials, calibration functions cannot be estimated in a "material-independent" way, but it is possible to determine the calibration coefficients using just three Finite Element calculations.

It should be noted that the nonlinear algorithm complements the linear one and does not replace it; in fact, even though it is capable of handling all orthotropic materials, it makes no sense to use a more complex and more CPU-intensive algorithm if the material does not require it. Moreover, the nonlinear algorithm needs a starting guess and uses an iterative approach, so that execution time is much longer than in the case of a linear one.

Regarding performances, both the numerical and experimental tests show the good reliability and accuracy of both the proposed algorithms whose results agree with high repeatability.

Appendix A. Numerical aspects

Estimating displacement fields using the theoretical solution requires some caution. In fact, Eqs. (10) and (11) are the result of multiple mapping (in particular affine mapping from the $x + \mathrm{i}y$ plane to the $x + \mu_i y$ plane followed by conformal mapping from the z_i plane to the ξ_i plane) where the latter, the inverse of $z_i = 1/2[(1 - \mathrm{i}\mu_i)\xi + (1 + \mathrm{i}\mu_i)\xi^{-1}]$, is particularly crucial. In fact, when going to the inverse function

$$\xi_i = \frac{z_i \pm \sqrt{z_i^2 - (1 + \mu_i^2)}}{1 - \mathrm{i}\mu_i}$$

one has to select the correct square root sign. Moreover, since both the μ_i and z_i are complex, the square root itself presents two poles, so spurious discontinuities may be generated in physical quantities if the correct numerical procedure is not followed.

To avoid these problems, one has first to rewrite the square root in such a way as to move the branch cut within the circular hole—so that it does not affect calculation—then select the correct sign. Skipping the theoretical aspects (Churchill, 1960), the first objective can be accomplished by first introducing the Z_i auxiliary variable

$$Z_i = \frac{z_i}{\sqrt{1 + \mu_i^2}}$$

and then estimating the square root as

$$\sqrt{z_i^2 - (1 + \mu_i^2)} = \pm\sqrt{1 + \mu_i^2}\sqrt{Z_i - 1}\sqrt{Z_i + 1}$$

To correctly choose the sign in front of square root, it is sufficient to check it at one point on the boundary of the hole, where the correct values are known (the inverse mapping reduces to $e^{-i\vartheta}$, see the end of Section 3), and then use the same sign through the calculation.

References

Baldi, A., 2005. A new analytical approach for hole drilling residual stress analysis by full field method. Journal of Engineering Materials and Technology 127 (2), 165–169.

Baldi, A., 2007. Full field methods and residual stress analysis in orthotropic material. I. Linear approach. International Journal of Solids and Structures 44 (25–26), 8229–8243.

Cárdenas-García, J.F., Ekwaro-Osire, S., Berg, J.M., Wilson, W.H., 2005. Non-linear least-square solution to the moiré hole method problem in orthotropic materials. Part I: Residual stresses. Experimental Mechanics 45 (4), 301–313.

Churchill, R.V., 1960. Complex Variables and Applications. McGraw-Hill (p. 82 ff).

Creath, K., 1993. Temporal phase measurement methods. In: Robinson, D.W., Reid, G.T. (Eds.), Interferogram Analysis: Digital Fringe Pattern Measurement Techniques, first ed. Institute of Physics Publishing, Bristol, UK; Philadelphia, US, pp. 94–140 (Chapter 4).

Jones, R.M., 1975. Mechanics of Composite Materials, international student ed. Scripta Book Company, Washington, DC.

Lekhnitskii, S.G., 1963. Theory of Elasticity of an Anisotropic Elastic Body. Holden-day (translation of 1950 Russian ed.).

Lekhnitskii, S.G., 1968. Anistropic Plates. Gordon and Breach Science Publisher (translation of 1957 Russian ed.).

Press, W.H., Teukolsky, S.A., Vetterling, W.T., Flannery, B.P., 1992. Numerical Recipes in C. The Art of Scientific Computing, second ed. Cambridge University Press.

Savin, G.N., 1961. Stress Concentration Around Holes. Pergamon Press (translation of 1951 Russian ed.).

Schajer, G.S., Yang, L., 1994. Residual-stress measurement unorthotropic materials using the hole-drilling method. Experimental Mechanics 34 (4), 324–333.

Schimke, J., Thomas, K., Garrison, J., 1968. Approximate Solution of Plane Orthotropic Elasticity Problems. Management Information Services, Detroit, MI.

Smith, C.B., 1944. Effect of elliptic or circular holes on the stress distribution in plates of wood or plywood considered as orthotropic materials. Technical Report Mimeo 1510. USDA Forest Products Laboratory, Madison, WI.

Tan, S.C., 1988. Finite-width correction factors for anisotropic plate containing a central opening. Journal of Composite Materials 22 (11), 1082–1105.